Single Antenna Passive Synthetic Aperture DoA Estimation

Leandro Geraldo da Costa, Daniele Oliveira Silva, and Felix Antreich
Department of Telecommunications, Aeronautics Institute of Technology (ITA), São José dos Campos, Brazil

***Abstract*— Direction-of-Arrival (DoA) estimation is critical for various applications such as radar, sonar, and wireless communication, where the identification of radio frequency (RF) source localization is essential. This paper presents a passive detection technique using a synthetic aperture with a single sensor element. The method leverages the sensor's movement to form a synthetic aperture, reducing system complexity and cost while maintaining high accuracy. Simulation results demonstrate the technique's effectiveness under different conditions, showing its potential for practical applications in surveillance, navigation, and RF interference detection and suppression.**

***Keywords*— Direction-of-Arrival, Synthetic Aperture, Passive Detection**

I. Introduction

Direction-of-Arrival (DoA) estimation is a critical aspect in various wireless communication and positioning applications. It is essential for identifying the location of radio frequency (RF) sources, such as in radar, sonar, indoor localization, and spatial-aware device localization. Traditional DoA estimation techniques typically rely on multi-antenna arrays, which are impractical for portable electronic devices due to their large form factor and complexity [1]. This challenge has led to the development of novel approaches using virtual antenna arrays and synthetic aperture techniques to achieve high-resolution and high-precision source localization with simple hardware configurations, as discussed in [2].

Recent advancements include the use of a single moving receiver in a synthetic aperture positioning (SAP) system. This approach compensates for nonlinear phase variations caused by platform movement and performs coherent accumulation of long-duration data, enhancing positioning accuracy even at a low signal-to-noise ratio (SNR). Similarly, the virtual antenna array concept leverages the movement of a single-antenna receiver to create multiple virtual array elements along its trajectory, capturing signal samples at different positions. This method reduces system complexity and cost using inexpensive, off-the-shelf hardware while maintaining high DoA estimation accuracy through robust signal processing algorithms, as shown in [3] and [4].

Building on these foundations, our research focuses on maximum likelihood (ML) DoA estimation for a uniform linear virtual array (ULVA) with a single sensor element. Each signal sample is collected only once at each position, determined by the inertial sensor of an moving airborne system or a compact satellites in low earth orbit. The proposed signal model estimates phase differences caused by the distance between successive signal collection points and compensates for phase variations caused by the travel time between these points, corresponding to the time sampling. We consider detection of a basic pulsed radar signal with a single omnidirectional antenna, allowing for the assessment of performance under various scenarios, including different numbers of collection points, receiver-radar distances, and carrier frequencies.

Our approach aims to enhance passive detection capabilities in airborne systems and CubeSat payloads by integrating inertial sensor data with advanced signal processing techniques, providing a cost-effective solution for accurate DoA estimation in portable and constrained environments. The performance evaluation through simulations demonstrates the effectiveness of the synthetic aperture with a single sensor element in two operational conditions, paving the way for practical implementations in surveillance, navigation, and RF interference suppression applications.

Leandro Geraldo da Costa, geraldolgc@ita.br; Daniele Oliveira Silva, daniele19954@gmail.; Felix Antreich, fean@ita.br. This work was partially supported by the Brazilian National Council for Scientific and Technological Development (CNPq) under grant 312394/2021-7 PQ-2, 406517/2022-3, 407245/2022-7, and 163978/2022-0, and by Brazil´s Funding Authority for Studies and Projects (FINEP) under grant 01.22.0581.00.

II. Sensing Scenario

The sensing scenarios examined in this work are depicted in Fig. 1 and Fig. 2. In both scenarios, we assume that the passive detection system moves at a constant velocity along the x-axis of a Cartesian coordinate system (xyz), starting from the origin and moving in the positive x direction with a fixed elevation angle of $\theta = 90°$.

A. Far-Field Assumption

Under the far-field assumption, as illustrated in Fig. 1, the received signal is assumed to arrive at each reception or sampling point $\mathbf{P}_n$ at discrete time intervals nT_s, where T_s is the sampling duration and $n = 0, 1, \ldots, N$. The unit vector $\vec{u}$, which is perpendicular to the incident planar wavefront, indicates the direction of the incoming signal at the initial position $\mathbf{P}_0$. The azimuth angle φ, defined as the DoA, is measured from the x-axis towards the y-axis, intersecting the vector $\mathbf{u}$.

As the distance between successive sampling points is small, all points $\mathbf{P}_n$ are expected to receive the incident planar wavefront at nearly the same azimuth angle φ. This can be achieved through a high sampling rate, ensuring that the spatial displacement between consecutive points remains small and with uniform distance Δ. When the distance Δ is uniform for all n, the steering vector can be represented as a Vandermonde vector. This representation is crucial in array signal processing, as it facilitates efficient and accurate DoA estimation.

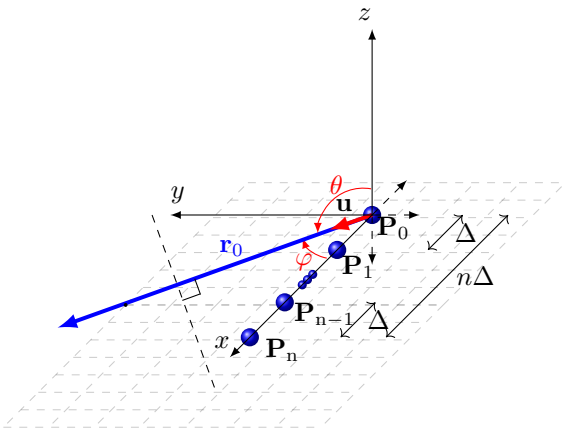

Fig. 1: Synthetic aperture sensing scenario for far-field assumption.

The time delay of the arriving signal at each sampling point relative to $\mathbf{P}_0$ can be given by

$$\begin{aligned}\tau_n &= -\frac{1}{c}\cos(\varphi)\|\mathbf{P}_n - \mathbf{P}_0\|_2 \\ &= -\frac{1}{c}\cos(\varphi)n\Delta, \end{aligned} \tag{1}$$

where φ is approximately constant across all n due to the far-field assumption, and $c = \lambda f_c$ is the speed of light, where f_c is the carrier frequency and λ is the respective wavelength of the received wavefront.

B. Spherical Wave Propagation

The far-field assumption in general is only full-filled if the distance between the transmitter and the receiver is very large and the number of reception points is limited (small synthetic aperture). Thus, in reality, spherical wave propagation has to be considered as illustrated in Fig. 2. Here, the time delay τ_n is directly related to the difference in travel time of the incident signal from the emitter to each sampling point compared to the time it takes to reach the reference point $\mathbf{P}_0$. Consequently, for spherical wave propagation, it is not possible to define a common angle of incidence φ for all points.

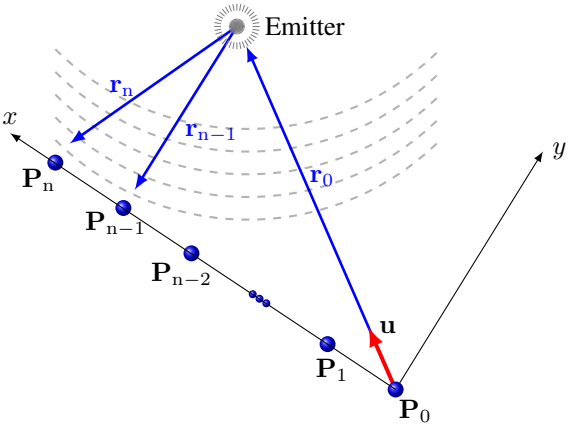

Fig. 2: Synthetic aperture scenario for spherical wave propagation.

The time delay τ_n of the arriving signal at each sampling point, for spherical wave propagation, is determined by the variation in the magnitude of the vectors $\mathbf{r}_n$ and $\mathbf{r}_0$, divided by the speed of light c and thus can be given as

$$\tau_n = \frac{\|\mathbf{r}_n\|_2 - \|\mathbf{r}_0\|_2}{c}. \tag{2}$$

C. Phase difference in a uniform linear virtual array

In the proposed sensing scenario, where a single sensor element moves and collects signals over time, the time sampling T_s plays a crucial role in estimating the phase variation between successive sampling points. As illustrated in Fig. 3, if the expected phase ϕ_{P_n} at time $t = 0$ is denoted by α, the corresponding phase difference at each sampling point is given by $(nT_s + \tau_n)f_c$.

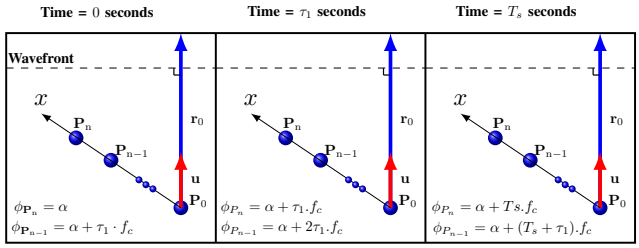

Fig. 3: Phase difference between consecutive sampling points of a passive detection system that moves at a constant velocity along the x-axis of a Cartesian coordinate system (xyz) under the assumptions of narrow band and far field.

III. Received Signal Data Model

Considering a sensing scenario as described in Fig. 1 and the far-field assumption, the received baseband signal at receiving point $\mathbf{P}_n$ can be expressed

$$y(t) = s(t - \tau_n)e^{-j2\pi f_c(\tau_n + nT_s)} + n(t) \tag{3}$$

where $n(t)$ is complex white Gaussian noise with $\mathcal{CN}(0, \sigma_n^2)$. Assuming a uniform distance Δ between the different points p_n we can write

$$\tau_n = -\frac{1}{c}\cos(\varphi)n\Delta. \tag{4}$$

Assuming a constant movement of the antenna along the x-axis with velocity v_x, $\Delta = T_s v_x$, and with uniform sampling of the received signal with a sampling duration of T_s we can define the received signal as

$$\begin{aligned} y(nT_s) &= s(nT_s - \tau_n)e^{-j2\pi f_c(\tau_n + nT_s)} + n(nT_s) \\ &= s(nT_s - \tau_n)e^{j\frac{2\pi}{\lambda}n\Delta\cos(\varphi)}e^{-j2\pi f_c nT_s} + n(nT_s) \end{aligned} \tag{5}$$

where $y[n] = y(nT_s)$, $s[n] = s(nT_s)$, and $n[n] = n(nT_s)$.

Assuming that for Q consecutive time instances for any value of n, the difference between consecutive delays can be approximated as

$$\begin{aligned} \Delta(\tau) &\approx \tau_n - \tau_{n-1} \\ &\approx \tau_{n+1} - \tau_n \\ &\approx \dots \\ &\approx \tau_{n+(Q-1)} - \tau_{n+(Q-2)}. \end{aligned} \tag{6}$$

This relation holds for short time intervals between consecutive samples. Specifically, for Q consecutive samples, also the received signal can be approximated as

$$\begin{aligned} s[n] &\approx s[n+1] \\ &\approx s[n+2] \\ &\approx \dots \\ &\approx s[n+(Q-1)]. \end{aligned} \tag{7}$$

Thus, we can rearrange the received signal in a vector notation

$$\begin{aligned} \mathbf{y}[k] = &\underbrace{e^{j\frac{2\pi}{\lambda}kQ\Delta\cos(\varphi)}e^{-j2\pi f_c kQT_s}s[kQ]}_{=\tilde{s}[k]} \\ &\underbrace{\begin{bmatrix} 1 \\ e^{j\frac{2\pi}{\lambda}\Delta\cos(\varphi)} \\ e^{j\frac{2\pi}{\lambda}2\Delta\cos(\varphi)} \\ \vdots \\ e^{j\frac{2\pi}{\lambda}(Q-1)\Delta\cos(\varphi)} \end{bmatrix} \odot \begin{bmatrix} 1 \\ e^{-j2\pi f_c T_s} \\ e^{-j2\pi f_c 2T_s} \\ \vdots \\ e^{-j2\pi f_c (Q-1)T_s} \end{bmatrix}}_{=\mathbf{a}(\varphi, f_c, v_x, T_s)} \\ &+ \underbrace{\begin{bmatrix} n[kQ] \\ n[kQ+1] \\ n[kQ+2] \\ \vdots \\ n[kQ+(Q-1)] \end{bmatrix}}_{=\mathbf{n}[k]} \\ = &\,\mathbf{a}(\varphi, f_c, v_x, T_s)\tilde{s}[k] + \mathbf{n}[k] \in \mathbb{C}^{Q\times 1}, \end{aligned} \tag{8}$$

with $k = 0, 1, \dots, K$. Collecting K data vectors and considering the DoA φ is constant over KQ samples, we can write

$$\mathbf{Y} = \mathbf{a}(\varphi, f_c, v_x, T_s)\tilde{\mathbf{s}}^{\mathrm{T}} + \mathbf{N} \in \mathbb{C}^{Q\times K}, \tag{9}$$

where

$$\mathbf{Y} = [\mathbf{y}[0], \mathbf{y}[1], \dots, \mathbf{y}[K]], \tag{10}$$

$$\mathbf{N} = [\mathbf{n}[0], \mathbf{n}[1], \dots, \mathbf{n}[K]], \tag{11}$$

$$\tilde{\mathbf{s}} = [\tilde{s}[0], \tilde{s}[1], \dots, \tilde{s}[K]]^{\mathrm{T}}. \tag{12}$$

IV. DoA Estimation

In this work we apply a maximum likelihood (ML) Doa estimator, which for a single impinging wavefront is equivalent with the so-called conventional beamformer applied to DoA estimation [5]. The signal vector $\mathbf{y}[k]$ can be considered to be of the general case described in [5] since it can be considered a realization of a random variable with some covariance matrix.

The covariance matrix $\mathbf{R}_{\mathbf{yy}}$ is estimated using $Q \times K$ samples [5]

$$\hat{\mathbf{R}}_{\mathbf{yy}} = \frac{1}{K}\sum_{k=1}^{K}\mathbf{y}[k]\mathbf{y}^{\mathrm{H}}[k] \in \mathbb{C}^{Q\times Q}. \tag{13}$$

We can also write

$$\hat{\mathbf{R}}_{\mathbf{yy}} = \frac{1}{K}\mathbf{Y}\mathbf{Y}^{\mathrm{H}} \in \mathbb{C}^{Q\times Q}. \tag{14}$$

The ML DoA estimator in the single-source case can be given as [5]

$$\hat{\varphi} = \arg\max_{\varphi}\left\{\mathbf{a}^{\mathrm{H}}(\varphi, f_c, v_x, T_s)\hat{\mathbf{R}}_{\mathbf{yy}}\mathbf{a}(\varphi, f_c, v_x, T_s)\right\} \tag{15}$$

Thus, the DoA estimation is obtained by maximizing the quadratic form of the steering vector and the covariance matrix. Simple line-search methods can be used to effectively solve this problem. For the estimation of the covariance matrix $\mathbf{R}_{\mathbf{yy}}$ also recursive methods can be derived in order to achieve a continuous updating scheme.

V. Simulations and Analysis

The simulations presented in this work were conducted using MATLAB to model a pulsed radar system, characterized by the coherent emission of signals through an omnidirectional antenna operating at two different carrier frequencies f_c. The passive detection system's receiver was modeled in continuous motion, maintaining constant velocity, altitude, and direction throughout the simulation period, starting from a known distance to the radar. To reduce the complexity of the 3D real-world scenario, both the radar and the receiver were positioned in the same xy-plane, with the elevation angle θ set to 90º. This simplification to a 2D problem was intentionally chosen to facilitate the initial development and testing of the proposed signal model, making it more manageable to analyze the core concepts without the added complexity of a full 3D model.

The system's performance was then evaluated under two distinct scenarios to assess its versatility and robustness. In the first scenario an airborne system was simulated, characterized by relatively low speed, shorter distance between radar and receiver, and lower carrier frequency f_c. Here, the sensor moved at $v_x = 100$ m/s with an initial line-of-sight distance of 1250 meters from the radar to the receiver, operating at a carrier frequency $f_c = 1$ GHz. In contrast, the second scenario modeled a CubeSat in low Earth orbit, where the conditions were significantly more demanding. The CubeSat was moving at a high velocity $v_x = 8000$ m/s with an initial line-of-sight distance of 500 kilometers from the radar to the receiver, and we considered a much higher carrier frequency $f_c = 26$ GHz.

These simulations were designed to demonstrate the system's capability across a wide range of operating conditions, from the relatively benign, low-speed, and low-frequency airborne environment to the more challenging, high-speed, and high-frequency spaceborne environment typical for CubeSat operations. The results from these simulations are used to validate the effectiveness of the proposed technique in both scenarios, underlining its potential applicability across various platforms, from airborne systems to CubeSats in low Earth orbit.

To ensure that the simulation results accurately reflected the performance of the proposed technique, the sensor element in the passive detection system was not subjected to any gain adjustments, and no errors were introduced in the estimation of position, time sampling, or phase of the received signal. This setup was deliberately chosen to isolate the performance of the technique from any external influences, providing clear insights to its capabilities.

Summarizing, the simulation parameters for the two described scenarios are listed in Tab. I.

In both scenarios, the received baseband signal considered for DoA estimation via the ML estimator was modeled considering the far-field assumption. This assumption simplifies the estimation process by considering that the signal arrives

TABLE I: Simulation parameters.

Parameter	Value
Simulated DoA	0:5:90 degrees
$\|\|\mathbf{r}_0\|\|_2$	1250 m (Airborne) or 500 km (CubeSat)
v_x	100 m/s (Airborne) or 8000 m/s (CubeSat)
SNR	0:5:50 dB
Q	[2,4,6,8,10,12,14,16,18,20,40,80,100,500,1000]
K	[1,10,20,30,40,50,100,200,500,1000]
f_c	1 GHz (Airborne) or 26 GHz (CubeSat)
T_s	0.025 μs
Monte Carlo runs	1000

at each sampling point with a nearly constant azimuth angle φ. This simplification is particularly useful in reducing the complexity of the estimation process, making it feasible to handle large datasets and multiple iterations.

However, to ensure greater precision in how the signal is actually received, the incoming signal at each sampling point was generated considering spherical wave propagation. This approach captures the true nature of the wavefront as it propagates, accounting for the varying distances between the radar and the receiver at each point. Hence, the simulations consider real-world propagation scenario considering a simplified signal model in the receiver for DoA estimation to reduce complexity.

A. DoA estimation for different SNRs, Q = 2, and K = 1

Fig. 4 presents the results from the low Earth orbit scenario, characterized by high velocity (8000 m/s) and $f_c = 26$ GHz. This graph is a combined bar chart displaying the Root Mean Square (RMS) DoA estimation error for different SNR, with Q = 2 and K = 1. The SNR values vary from 0 to 50 dB in increments of 5. The bars within each SNR group represent the RMS DoA estimation error for different DoA azimuth angles φ, ranging from 0º to 90º in 5º increments, with the RMS estimation error of the lower φ being represented by the first bars on the left side of each group of bars.

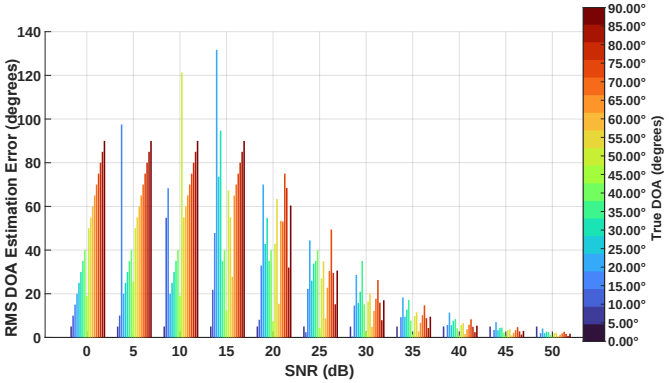

Fig. 4: RMS DoA estimation error dependent on the SNR and the true DoA azimuth angle (low Earth orbit scenario, $Q = 2$, $K = 1$)

This chart illustrates the worst-case scenario for applying the ML DoA estimator due to the minimal configuration of the uniform linear virtual array (ULVA) with Q = 2 and K = 1. A clear pattern emerges in the group of SNR $= 0$, where the RMS error increases with the true DoA angle. This is because the estimated DoA remains near 0º across all simulations, while the real DoA increases from 0º to 90º, causing the RMS error to rise proportionally. Essentially, there is no effective DoA detection in the group of SNR $= 0$, with the highest RMS error occurring at 90º.

As the SNR improves from 5 to 15 dB, some DoA angles begin to show estimatied angles different from 0º, leading to deviations from the error pattern observed in the SNR 0 dB group. By SNR 20 dB, the system begins to offer some meaningful DoA estimates, though the errors remain significant. Despite the challenges presented by this scenario, at higher SNR levels (above 30 dB), the RMS DoA estimation error for all DoA azimuth angles φ remains below 20º, indicating some level of usable detection even in this challenging configuration.

B. RMS DoA estimation error for SNR = 0 dB

Fig. 5 presents a box plot that illustrates the RMS DoA estimation error for an SNR of 0 dB, focusing on the relationship between increasing the number of data snapshots K considering a fixed Q. In this case, Q is set to 20, and various values of K are explored to demonstrate how increasing K can significantly improve DoA estimation accuracy, even in challenging low SNR conditions.

Each box plot represents the distribution of the RMS estimation error calculated across all possible DoA azimuth angles φ, ranging from 0º to 90º, for a specific value of K. This means that the spread, quartiles, and median in each box plot reflect the performance of the ML DoA estimation method over the entire range of possible angles, providing a comprehensive overview on the estimation performance.

The box plot reveals that with $Q = 20$ and $K = 10$, the third quartile of the RMS DoA estimation error is under 10°, and the median error is 5.5°. This result is already promising, as it indicates that even at a very low SNR, useful DoA estimates can be achieved. In fact, these results are often better than those obtained using other DoA estimation techniques, such as amplitude comparison methods.

As K increases to 1000, the performance further improves, with the median RMS DoA estimation error dropping to 0.70°, and all outliers falling below 10°. This significant reduction in error highlights the value of increasing K for a given Q, even under low SNR conditions. The results demonstrate that, by adequately increasing the number of data snapshots, the ML DoA estimator can achieve high accuracy, making it a viable option even when the signal environment is less than ideal.

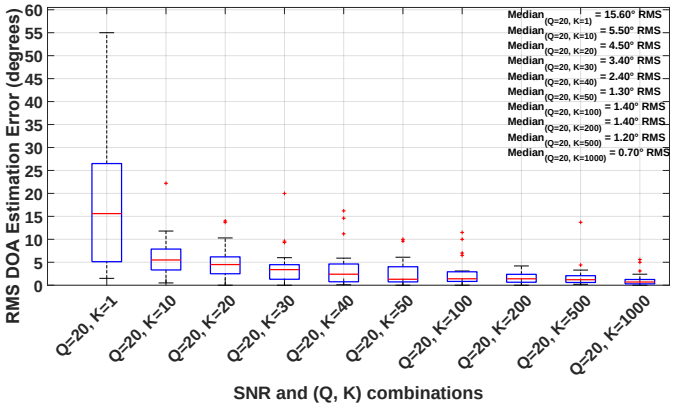

Fig. 5: Box plot of RMS DoA estimation error for increasing K at SNR = 0 dB (low Earth orbit scenario, $Q = 20$)

C. Airborne scenario with low velocity and carrier frequency

Fig. 6 presents the results from the airborne scenario with a velocity of 100 m/s and $f_c = 1$ GHz, where the receiver was positioned at a line-of-sight distance of 1250 meters from the radar. The evaluation was conducted using the minimum configuration for DoA estimation with a ULVA, using $Q = 2$ and $K = 1$, expected to yield the poorest performance compared to configurations with higher Q or K.

Interestingly, the pattern observed in the SNR 0 group of the low Earth orbit scenario with minimal Q and K reappears here across all SNR levels. The RMS DoA estimation error shows little variation related to SNR groups, increasing linearly with the DoA azimuth angle φ and peaking at 90º, similar to the low Earth orbit scenario at SNR 0.

This consistency suggests that across all simulation iterations, the system estimates the DoA as 0º regardless of the actual DoA, causing the RMS DoA estimation error to rise as the DoA diverges from 0º. This behavior indicates that with the minimal configuration of $Q = 2$ and $K = 1$, the ML DoA estimation method cannot provide any useful results.

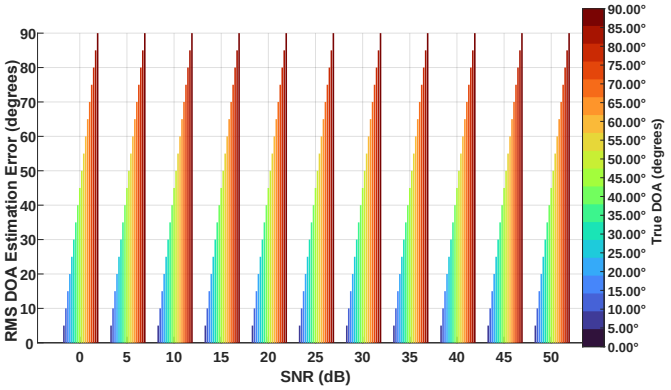

Fig. 6: RMS DoA estimation error dependent on the SNR and the DoA azimuth angle (airborne scenario, $Q = 2$, $K = 1$)

Similar to Fig. 5, Fig. 7 presents a box plot that illustrates the RMS DoA estimation error at an SNR of 0 dB, focusing on how the number of data snapshots K affects estimation accuracy when Q is fixed. In this scenario, Q must be set to 1000 before the ULVA begins to provide reasonably accurate DoA estimates. By exploring various values of K, the plot demonstrates that increasing K can significantly enhance DoA estimation accuracy, even in challenging low SNR environments.

As K increases to 1000, the performance improves dramatically. The median RMS DoA estimation error decreases from 37° to 2.80°, with all outliers falling below 20°. This substantial reduction in error highlights the importance of increasing K for a given Q, even under low SNR conditions. The results indicate that, with a sufficiently high Q value, increasing the number of data snapshots allows the ML DoA estimator to achieve high accuracy, making it a reliable option even in less-than-ideal signal environments.

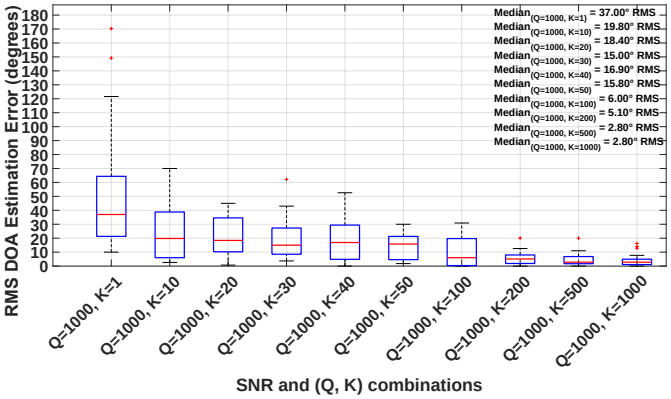

Fig. 7: Box lot of RMS DoA estimation error for increasing K at SNR = 0 dB (airborne scenario, $Q = 1000$)

VI. Conclusion

This paper presented a novel approach to DoA estimation using a single antenna in a ULVA configuration. By leveraging the movement of the sensor to create a synthetic aperture, the method achieves high-accuracy DoA estimation while minimizing system complexity. Simulations conducted in both airborne and CubeSat scenarios demonstrated the technique's effectiveness, with the scenarios reduced to a 2D problem to simplify analysis.

In the CubeSat scenario, characterized by high velocity and high-frequency conditions, the simulations showed that the proposed method could provide useful DoA estimates even in challenging environments with the minimal configuration $Q = 2$ and $K = 1$ (single snapshot). However, performance significantly improved with an increase in the number of data snapshots (K), highlighting the importance of adequately configuring K to achieve reliable results.

Similarly, in the airborne scenario, which involved lower velocity and carrier frequency, the simulations indicated that the ULVA configuration with minimum settings of $Q = 2$ and $K = 1$ could struggle to produce accurate DoA estimates. Nevertheless, as K and Q were increased, the method's accuracy improved significantly, reducing the RMS DOA estimation error and demonstrating its potential even in less-than-ideal conditions.

Overall, the results validated the proposed DoA estimation technique's versatility and robustness. By adjusting the parameters Q and K, the method can be tailored to various operational scenarios, making it a viable option for applications ranging from low-speed airborne platforms to high-speed CubeSats in low Earth orbit. The reduction of these scenarios to a 2D problem not only facilitated the initial development and testing but also provided a clear and manageable framework for demonstrating the core concepts of the proposed technique without loss of generality.

References

[1] H. L. V. Trees, *Optimum Array Processing. Detection, Estimation and Modulation Theory, Part IV*. Wiley Interscience, 2002.

[2] J. Cheng, K. Guan, and F. Quitin, "Direction-of-arrival estimation with virtual antenna array: Observability analysis, local oscillator frequency offset compensation, and experimental results," *IEEE Transactions on Instrumentation and Measurement*, vol. 70, pp. 1–13, 2021.

[3] Y. Wang, G.-C. Sun, Y. Wang, Z. Zhang, M. Xing, and X. Yang, "A high-resolution and high-precision passive positioning system based on synthetic aperture technique," *IEEE Transactions on Geoscience and Remote Sensing*, vol. 60, pp. 1–13, 2022.

[4] F. Quitin, P. De Doncker, F. Horlin, and W. P. Tay, "Virtual multiantenna array for estimating the direction of a transmitter: System, bounds, and experimental results," *IEEE Transactions on Vehicular Technology*, vol. 67, no. 2, pp. 1510–1520, 2018.

[5] N. O'Donoughue, *Emitter Detection and Geolocation for Electronic Warfare*, ser. Artech House electronic warfare library. Artech House, 2019. [Online]. Available: https://books.google.com.br/books?id=TbjEDwAAQBAJ